

Isotropic and Anisotropic Interfaced Lambertian Microfacets

Daniel Meneveau, Benjamin Bringier, Emmanuelle Tauzia,
Mickaël Ribardière, Lionel Simonot

December 18th, 2015

Abstract

Specular microfacet distributions have been successfully employed by many authors for representing materials glossiness, and they are generally combined with a Lambertian term that accounts for the colored aspect. Such a representation makes use of the Fresnel *reflectance* factor at the interface, but the *transmission* factor is often ignored. In addition, the generalization to microfacet distributions with a more general reflectance is known to be complex, since it requires to solve an angular integral that has no analytical solution. This paper proposes a complete framework for physically handling both reflection and transmission with microfacet distributions. First, we show how transmission affects reflectance of an *interfaced Lambertian* model, and provide an analytical description of an individual microfacet reflectance. Second, we describe a method for handling distributions of such microfacets in any physically based Monte-Carlo rendering systems, as well as an approximate representation (which includes light multiple reflexions based on V-cavities representation) that can be used for GPU applications or for measured data fitting. Our approach generalizes several previous models, including flat Lambertian materials as well as specular and Lambertian microfacets. The result section illustrates the wide range of materials that can be possibly taken into account with this representation.

1 Introduction

Realistic and physically plausible representations of reflectance have been studied for a long time in optics and computer graphics. Yet, many questions still remain open because the mathematical models dedicated to Bidirectional Reflectance Distribution Functions (BRDFs) must fulfill various requirements, such as physical plausibility, ability to naturally represent existing/measured materials, visual realism, computation time efficiency for producing computer generated images, material control for users and artists, etc.

The wide variety of empirical models, introduced for instance by Phong [1], Blinn-Phong [2], or the revised version proposed by Lewis [3], offers a competitive and intuitive way to define surface optical properties, but the parameters used do not correspond to actual physical characteristics and they have limited expressiveness. Other approaches favor function bases whose coefficients can be obtained from measurements using projection or parameter fitting, e.g. with wavelets [4], spherical harmonics [5], or Phong lobes [6]. Unfortunately with such representations, both the nature and the large number of coefficients make it difficult for users to tune material appearances manually. Finally, *physically based* BRDF models [7–14] are often preferred because they are defined by parameters that correspond to physical aspects of materials, such as surface roughness, chromaticity, or refractive indices. Many of them rely on a statistical distribution of microfacets associated with their reflectance property.

BRDFs based on microfacet distributions have been introduced in computer graphics for the representation of glossy reflections on rough surfaces [7, 15]. The formulation corresponds to a product of Fresnel reflectance, distribution and attenuation factors. Materials can be metallic (complex refractive index), highly reflecting light [16, 17], or dielectric (real refractive index) which only partly reflect light. In this latter case, transmission should be accounted for. For instance, Walter *et al.* [11] propose to

handle refraction of rough transparent dielectrics. With paints, plastics, ceramics, and so on, light goes through the dielectric interface and scatters within the material body before re-exiting the surface. In most models, this effect is approximated using a Lambertian term that does not depend on the specular aspect of the surface.

However, as pointed out by several authors, the matte component of rough materials is not constant and often exhibit backscattering [9, 18, 19]. The Lambertian term should at least account for BRDF specular albedo to deduce the remaining body reflectance behavior [20, 21]. Though physically plausible, this latter representation does not explicitly correlate reflectance with the substrate roughness, and backscattering is not handled.

Simonot [22] introduces *interfaced Lambertian microfacets* for physically handling the transmission through a Fresnel interface and multiple reflections with a Lambertian substrate. This theoretical model has been originally defined with a Gaussian distribution of normals, without taking masking and shadowing into account, and numerical integration is required because microfacets are not only specular.

In this paper, we extend Simonot’s work and make it possible to use interfaced Lambertian microfacets in rendering systems. We render the effects of this model, and confront the obtained results with other microfacet-based BRDFs. Figure 1 illustrates some results produced with the approaches described in this paper. While Jakob *et al.* [12] define materials explicitly with rough translucent layers, interfaced Lambertian microfacets are closer to Oren and Nayar’s approach [9], and handle backscattering. In our case, contrary to Jakob *et al.*, explicit lighting simulation within layers is not required since inter-reflections between the substrate and the interface are analytically described. Our representation can be directly integrated in any Monte-Carlo based lighting simulation renderer, and we also propose an approximate model which includes light multiple reflections within V-cavities.

More specifically, the contributions of this paper consist of:

- a consistent framework dedicated to microfacet BRDFs, that integrates a homogeneous matte body with a rough interface; it extends previous models for opaque materials, including flat specular or Lambertian, as well as a range from specular to Lambertian rough surfaces, with various distributions;
- a practical solution for straightforwardly integrating such models within Monte-Carlo-based rendering systems, including importance sampling and anisotropy;
- a method based on path tracing for handling light multiple reflection contributions within V-cavities;
- an approximate model that can be employed for direct lighting, GPU, and measurement fitting, based on the Oren-Nayar representation, and which handles light inter-reflections between microfacets.

Our results show that this model accounts for many reflection phenomena, including backscattering, anisotropy, and BRDF darkening at incoming and outgoing grazing angles, that can be observed on some measured materials. These effects are naturally included in the model since it physically handles balance between specular and body reflections.

The remainder of the paper is organized as follows. Section 2 presents the theory of microfacet BRDF models and introduces notations. Section 3 describes interfaced Lambertian microfacet BRDFs. Section 4 explains how scattering microfacets can be employed in various configurations in rendering systems. Section 5 presents our results for various cases, including comparisons and fittings from measured BRDFs. Conclusion and future work are provided in Section 6.

2 Microfacet-Based BRDF

This paper focuses on microfacet-based models for *opaque* materials, as described by Torrance and colleagues [7, 15], Oren and Nayar [9], Ashikhmin *et al.* [10], Bagher *et al.* [23], Dupuy *et al.* [24], or Heitz [25]. They have been successful at representing various families of materials with only a few parameters clearly related to surface observations and intuitive to manipulate. So far, they have been described using (i) a microfacet distribution, (ii) an elementary reflectance (purely specular or Lambertian), and (iii) geometric factors accounting for light shadowing and masking.

2.1 Definitions and Notations

The notations used in this paper are given in Table 1, they correspond to those proposed by Nicodemus *et al.* [26]. Any direction \mathbf{u} is defined with a polar angle θ_u and an azimuthal angle φ_u expressed according to the macrosurface normal \mathbf{n} .

Let us consider a surface sample of normal \mathbf{n} lit by a collimated light source, from direction \mathbf{i} , as illustrated in Figure 1. The radiance reflected toward an observer \mathbf{o} is given by the BRDF $f(\mathbf{i}, \mathbf{o}, \mathbf{n})$. It is defined as the ratio between the elementary radiance $dL(\mathbf{i}, \mathbf{o}, \mathbf{n})$ reflected by the surface in direction \mathbf{o} and the incident irradiance $dE(\mathbf{i}, \mathbf{n})$ coming from direction \mathbf{i} :

$$f(\mathbf{i}, \mathbf{o}, \mathbf{n}) = \frac{dL(\mathbf{i}, \mathbf{o}, \mathbf{n})}{dE(\mathbf{i}, \mathbf{n})}. \quad (1)$$

A BRDF should be *physically plausible*, i.e. should satisfy Helmholtz reciprocity, i.e. $f(\mathbf{i}, \mathbf{o}, \mathbf{n}) = f(\mathbf{o}, \mathbf{i}, \mathbf{n})$ and energy conservation, i.e. $\int_{\Omega_+} f(\mathbf{i}, \mathbf{o}, \mathbf{n}) |\mathbf{on}| d\omega_o \leq 1, \forall \mathbf{i} \in \Omega_+$, with $|\mathbf{on}| = \mathbf{on}$ if $\mathbf{on} > 0$ and 0 otherwise.

The microfacet representation of a BRDF $f(\mathbf{i}, \mathbf{o}, \mathbf{n})$ corresponds to a statistical description of microfacet distribution. Given the BRDF $f^\mu(\mathbf{i}, \mathbf{o}, \mathbf{m})$ of an individual microfacet associated with normal \mathbf{m} , its contribution is weighted by the distribution $D(\mathbf{m})$ and a geometric attenuation factor (or GAF) $G(\mathbf{i}, \mathbf{o}, \mathbf{m})$. The distribution function $D(\mathbf{m})$ defines the surface roughness, indicating the proportion of microfacets oriented according to a given orientation \mathbf{m} ; the attenuation factor $G(\mathbf{i}, \mathbf{o}, \mathbf{m})$ determines the portion of a microfacet of normal \mathbf{m} visible from both the light source and the observer, with a major influence at grazing angles. Many authors have studied the use of various distributions and geometric attenuation factors [7, 9–11, 15, 20, 23, 24, 27], which have to be carefully chosen together [10, 25]:

$$f(\mathbf{i}, \mathbf{o}, \mathbf{n}) = \int_{\Omega_+} \frac{|\mathbf{im}|}{|\mathbf{in}|} f^\mu(\mathbf{i}, \mathbf{o}, \mathbf{m}) \frac{|\mathbf{om}|}{|\mathbf{on}|} D(\mathbf{m}) G(\mathbf{i}, \mathbf{o}, \mathbf{m}) d\omega_m. \quad (2)$$

All microfacets are supposed to be oriented in the upper hemisphere, with $D(\mathbf{m}) = 0$ if $\mathbf{mm} \leq 0$; the projected areas of all microfacets have to be equal to the macroscopic surface, i.e. $\int_{\Omega_+} D(\mathbf{m}) |\mathbf{mn}| d\omega_m = 1$.

In the case of purely specular microfacets, Equation 2 simplifies to [7, 11, 15]:

$$f(\mathbf{i}, \mathbf{o}, \mathbf{n}) = \frac{F(\mathbf{i}, \mathbf{h}) D(\mathbf{h}) G(\mathbf{i}, \mathbf{o}, \mathbf{h})}{4 |\mathbf{ih}| |\mathbf{oh}|}, \quad (3)$$

where $\mathbf{h} = \frac{\mathbf{i} + \mathbf{o}}{|\mathbf{i} + \mathbf{o}|}$ is the half angle vector between \mathbf{i} and \mathbf{o} , and $F(\mathbf{i}, \mathbf{h})$ corresponds to Fresnel reflectance, depending on the medium refractive index n_i (see Table 1). This equation defines the *glossy* aspect of the surface.

2.2 Discussion

On the one hand, rough metallic surfaces are almost opaque (Fresnel reflectance values are close to 1), and n_1 is defined by a complex value, with reflectance variations according to wavelengths [16].

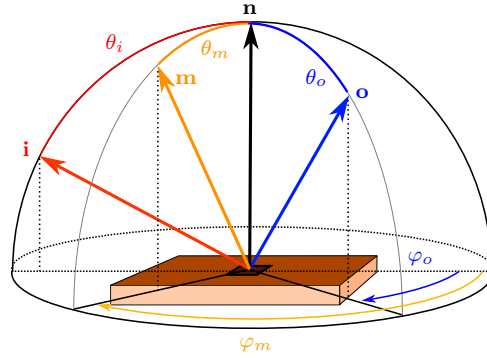


Figure 1: Geometry of reflection with our notation.

Table 1: *Notations used in this paper.*

\mathbf{n}	Macroscopic normal unit vector
\mathbf{m}	Microfacet normal unit vector
\mathbf{i}	Incident light unit vector direction
\mathbf{o}	Observer unit vector direction
\mathbf{h}	Half angle unit vector, bisector between \mathbf{i} and \mathbf{o}
θ_u	Polar angle associated with direction \mathbf{u}
φ_u	Azimuthal angle associated with direction \mathbf{u}
$d\omega_u$	Elementary solid angle around direction \mathbf{u}
Ω_+	Upper hemisphere of direction \mathbf{n}
$f(\mathbf{i}, \mathbf{o}, \mathbf{n})$	Macroscopic BRDF
$f^\mu(\mathbf{i}, \mathbf{o}, \mathbf{m})$	Microfacet BRDF
$D(\mathbf{m})$	Microfacet normal distribution
σ_x, σ_y	Roughness parameters given in local coordinate system for dealing with anisotropy
$G(\mathbf{i}, \mathbf{o}, \mathbf{m})$	Geometric attenuation factor
n_0	External refractive index
n_1	Internal refractive index
$n_i = \frac{n_1}{n_0}$	Ratio of refractive indices
$F(\mathbf{i}, \mathbf{m})$	Fresnel term, interface reflectance
$T(\mathbf{i}, \mathbf{m})$	Interface transmittance $T(\mathbf{i}, \mathbf{m}) = 1 - F(\mathbf{i}, \mathbf{m})$

Such materials are handled with specular microfacets directly since the resulting chromaticity and glossiness are completely handled by the Fresnel term and the chosen distribution. On the other hand, dielectrics correspond to real values of n_1 , with negligible wavelength dependency (the wavelength dependency is only related to body reflection). For common values of n_i (i.e. $1 \leq n_i < 3$), the Fresnel reflectance is low except at grazing angles. With energy conservation, the interface transmittance is significant although it is generally ignored [7] or roughly approximated [20]. The model presented in this paper handles this latter type of material and deals with transmission of light through the interface represented by a real refractive index and multiple light reflections between a Lambertian substrate and the interface.

The strong assumption of considering only pure Lambertian or pure specular microfacets restricts the gamut of materials that can be reproduced. For instance, the objects represented by the Oren-Nayar model [9] cannot exhibit any glossy appearance, while the Cook-Torrance model [7] only employs a constant Lambertian term, that does not account for backscattering with rough materials [9]. These models should not be combined for taking into account simultaneously glossy and matte aspects for three main reasons: first, Oren and Nayar use a distribution which is very rarely used in other models; second, interfaced Lambertian microfacets exhibit chromaticity variations according to the interface refractive index discontinuity, that cannot be handled using a simple combination of models; third, energy conservation is not handled with such a combination since body reflection should also depend on n_i .

The choice of $D(\mathbf{m})$, $G(\mathbf{i}, \mathbf{o}, \mathbf{m})$, and $f^\mu(\mathbf{i}, \mathbf{o}, \mathbf{m})$ may provide a wide range of physically plausible materials, as long as the combinations are carefully chosen [10, 11, 25, 27].

3 Interfaced Lambertian BRDF

The model presented in this paper defines rough surfaces (Figure 2) made up with a Lambertian substrate of parameter K_d (which depends on the wavelength λ), covered with a flat interface corresponding to a refractive index discontinuity n_i (a real index for dielectrics) between these two media. It accounts for both surface and body reflections.

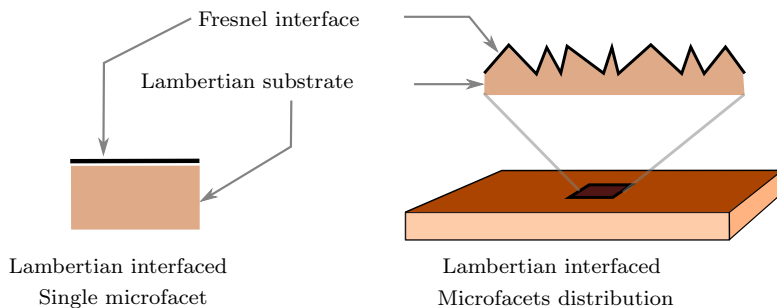


Figure 2: Surface built up with interfaced Lambertian microfacets. The substrate scatters light while the interface provides brightness.

3.1 Single Microfacet (or flat surface)

Interfaced Lambertian microfacets are associated with a BRDF $f^\mu(\mathbf{i}, \mathbf{o}, \mathbf{m})$ defined by a pure specular interface reflection $f_s^\mu(\mathbf{i}, \mathbf{o}, \mathbf{m})$ combined with the material volume body diffuse reflection $f_b^\mu(\mathbf{i}, \mathbf{o}, \mathbf{m})$:

$$f^\mu(\mathbf{i}, \mathbf{o}, \mathbf{m}) = f_s^\mu(\mathbf{i}, \mathbf{o}, \mathbf{m}) + f_b^\mu(\mathbf{i}, \mathbf{o}, \mathbf{m}). \quad (4)$$

Since microfacet interfaces are considered as perfectly flat, the surface reflection component $f_s^\mu(\mathbf{i}, \mathbf{o}, \mathbf{m})$

is [11]:

$$f_s^\mu(\mathbf{i}, \mathbf{o}, \mathbf{m}) = F(\mathbf{i}, \mathbf{h}) \frac{\delta\omega_m(\mathbf{h}, \mathbf{m})}{4|\mathbf{ih}|^2}, \quad (5)$$

where \mathbf{h} is the bissector direction of \mathbf{i} and \mathbf{o} , $\delta\omega_m$ is the dirac distribution associated with the elementary solid angle $d\omega_m$ around \mathbf{m} , so that for any solid angle Ω :

$$\int_{\Omega} \delta\omega_m(\mathbf{s}, \mathbf{m}) d\omega_m = \begin{cases} 1 & \text{if } \mathbf{s} \in \Omega \\ 0 & \text{otherwise} \end{cases} \quad (6)$$

and $F(\mathbf{i}, \mathbf{h})$ is the reflectance of the interface (for unpolarized irradiance), corresponding to the Fresnel's law between an outer medium of index n_0 and a medium of index n_1 :

$$F(\mathbf{i}, \mathbf{h}) = \frac{1}{2} \frac{(g-c)^2}{(g+c)^2} \left\{ 1 + \frac{[c(g+c)-1]^2}{[c(g-c)+1]^2} \right\}, \quad (7)$$

where $c = \mathbf{i} \cdot \mathbf{h}$ and $g^2 = n_i^2 + c^2 - 1$.

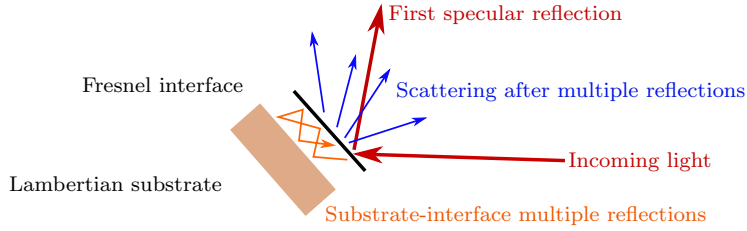


Figure 3: Interfaced microfacet body reflection: light is both reflected and transmitted by the interface. Our model also accounts for light multiple scattering.

Body scattering (Figure 3) should account for the first interface transmission $T(\mathbf{i}, \mathbf{m}) = 1 - F(\mathbf{i}, \mathbf{m})$ of light, followed by a Lambertian reflection due to the substrate (of reflectance K_d), inner multiple interactions between interface and substrate $1/(1 - K_d r_i)$, and final transmissions toward the outgoing direction, of transmittance $T(\mathbf{o}, \mathbf{m})$:

$$f_b^\mu(\mathbf{i}, \mathbf{o}, \mathbf{m}) = \frac{1}{\pi n_i^2} T(\mathbf{i}, \mathbf{m}) T(\mathbf{o}, \mathbf{m}) \frac{K_d}{(1 - K_d r_i)}, \quad (8)$$

where r_i is the internal reflectance on the flat interface lit by a Lambertian source coming from the medium of index n_i :

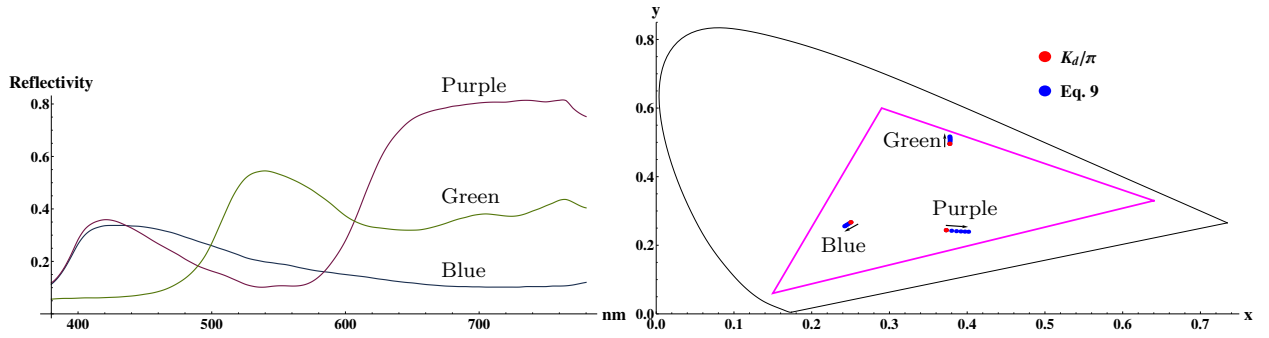
$$r_i = \int_{\theta_u=0}^{\pi/2} F_i(\mathbf{u}, \mathbf{m}) \sin(2\theta_u) d\theta_u, \quad (9)$$

with F_i the microfacet inner Fresnel reflectance. We use the analytical expression $n_i^2(1 - r_i) = 1 - r_e$ with r_e provided by Molenaar *et al.* [28]:

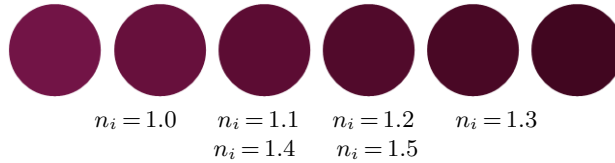
$$r_e = \frac{1}{2} - \frac{2n_i^3(n_i^2 + 2n_i - 1)}{(n_i^2 + 1)(n_i^4 - 1)} + \frac{(n_i - 1)(3n_i + 1)}{6(n_i + 1)^2} + \frac{8n_i^4(n_i^4 + 1)}{(n_i^2 + 1)(n_i^4 - 1)^2} \ln(n_i) + \frac{n_i^2(n_i^2 - 1)^2}{(n_i^2 + 1)^3} \ln\left(\frac{n_i - 1}{n_i + 1}\right) \quad (10)$$

This model considers an interface between two media, i.e. with a refractive index discontinuity, thus not subject to interferences.

With interfaced Lambertian microfacets in Equation 8, $1/n_i^2$ expresses an extension of the light beam from a medium of index n_1 to a less refringent medium of index $n_0 < n_1$. The multiple reflections between the interface and the substrate lead to chromatic variations depending on parameter n_i . Figure 4a provides three spectral reflectances of the Macbeth color checker corresponding to CIE xy values given in Figure 4b for normalized illuminant D65. This diagram shows that chromaticity



(a) Spectral reflectance $K_d(\lambda)$ for three colored samples. (b) Chromaticity variations for the three color checker samples given above and the color gamut PAL/SECAM, according to n_i for values equal to $n_i = \{1.0, 1.1, 1.2, 1.3, 1.4, 1.5\}$, with $\theta_i = 65^\circ$. The arrows illustrate the variation direction when n_i is increased.



(c) Visual aspect of chromaticity variations according to n_i for the purple sample, with PAL/SECAM color gamut and $\theta_i = 65^\circ$.

Figure 4: $K_d(\lambda)$ and chromaticity variations according to n_i , for three sample colors from the Macbeth color checker.

actually varies according to n_i , providing darker and more saturated colors. Figure 4c illustrates colored disks with these variations, according with n_i .

With achromatic objects, some variations are also noticeable, since increasing values of n_i also tend to provide higher transmission, and consequently darker body reflection. Figure 5 shows the curves and a rendered 3D object with materials corresponding to a flat interfaced Lambertian surface, with varying values of n_i . Light inter-reflections between the interface and the substrate affect the object appearance depending on $K_d/(1 - K_d r_i)$. Reflected radiance decreases when n_i increases, and when observation angles become grazing, contrary to Lambertian or rough Lambertian materials.

3.2 Rough Interfaced Lambertian BRDF

Using f^μ from Equation 4 in Equation 2, the global BRDF remains an expression composed of a glossy and a matte components (resp. f_s and f_b):

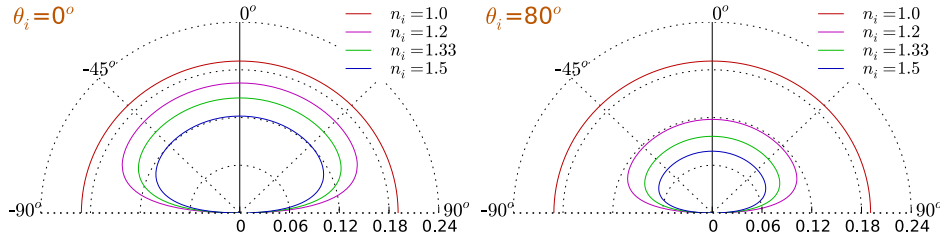
$$f(\mathbf{i}, \mathbf{o}, \mathbf{n}) = f_s(\mathbf{i}, \mathbf{o}, \mathbf{n}) + f_b(\mathbf{i}, \mathbf{o}, \mathbf{n}). \quad (11)$$

The specular component that provides glossiness, corresponds to Equation 3 (coming from Equations 2 and 5), while from Equations 2 and 8, the body reflection becomes:

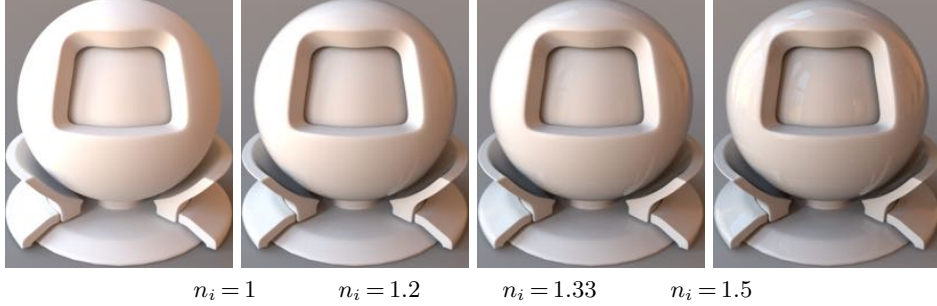
$$f_b(\mathbf{i}, \mathbf{o}, \mathbf{n}) = \frac{K_d}{\pi n_i^2 (1 - r_i K_d)} \times \int_{\Omega_+} T(\mathbf{i}, \mathbf{m}) T(\mathbf{o}, \mathbf{m}) D(\mathbf{m}) G(\mathbf{i}, \mathbf{o}, \mathbf{m}) \frac{|\mathbf{im}| |\mathbf{om}|}{|\mathbf{in}| |\mathbf{on}|} d\omega_m. \quad (12)$$

With this representation, several noticeable characteristics can be underlined:

- when $K_d = 0$, this formulation corresponds to purely specular microfacets;



(a) Body reflection according to refractive index (the specular reflection peak is not illustrated here since it only corresponds to a dirac).



(b) Rendered images of a flat interfaced Lambertian BRDF, with various values of n_i .

Figure 5: (a) BRDF of a flat interfaced Lambertian surface with $K_d = 0.6$ for each component r,v,b, and $n_i = \{1.0, 1.2, 1.33, 1.5\}$; (b) rendered images of the same BRDFs applied on a 3D object.

- when $n_i = 1$, then $T = 1$ and $r_i = 0$, it corresponds to purely Lambertian microfacets;
- when $\sigma = 0$, the BRDF is a flat interfaced Lambertian surface;
- when $n_i = 1$ and $\sigma = 0$, the model is equivalent to a flat Lambertian material.

In this paper, we have employed various distributions and geometric attenuation factors from the literature.

Gaussian distribution of normals is essentially used in the Oren-Nayar model [9]. This distribution is employed in this paper only for comparison purposes, with the following isotropic formulation:

$$D(\mathbf{m}) = C e^{(-\theta_m^2/2\sigma^2)} / |\mathbf{m}\mathbf{n}|, \quad (13)$$

where σ is the roughness parameter (expressed in radians) and $1/C = 2\pi \int_{\theta_m=0}^{\pi/2} e^{(-\theta_m^2/2\sigma^2)} \sin \theta_m d\theta_m$. Using such a distribution remains difficult in practice because of the estimation of C . The correspondance with Beckmann or GGX distributions requires $\sigma' = \sqrt{2}\sigma$. We employ this distribution as Oren and Nayar [9], in association with the Torrance-Sparrow geometric attenuation factor [15], which is mathematically well-posed [25]. This factor assumes V-cavities much longer than large:

$$G(\mathbf{i}, \mathbf{o}, \mathbf{m}) = \max\left(0, \min\left(1, \frac{2|\mathbf{i}\mathbf{n}||\mathbf{m}\mathbf{n}|}{|\mathbf{i}\mathbf{m}|}, \frac{2|\mathbf{o}\mathbf{n}||\mathbf{m}\mathbf{n}|}{|\mathbf{o}\mathbf{m}|}\right)\right). \quad (14)$$

However, this assumption is somehow physically unrealistic and prone to discontinuities at grazing angles.

Beckmann distribution is often referenced in the literature [7, 10, 20]. It corresponds to a Gaussian distribution of microfacet slopes. Ward [8] proposes a derived anisotropic distribution, and Kurt *et al.* [13] provides the following formulation, that includes the correct normalization:

$$D(\mathbf{m}) = \frac{e\left(-\tan^2 \theta_m \left(\frac{\cos^2 \varphi_m}{\sigma_x^2} + \frac{\sin^2 \varphi_m}{\sigma_y^2}\right)\right)}{\pi \sigma_x \sigma_y |\mathbf{m}\mathbf{n}|^4} \quad (15)$$

where σ_x and σ_y correspond to the roughness parameters (standard deviations of slopes) associated with a local coordinate system. The well-known Cook-Torrance model corresponds to the isotropic

form of this distribution (for $\sigma_x=\sigma_y$), associated with the Torrance-Sparrow GAF. Several authors have discussed attenuation factors [10,25,29] since the Torrance-Sparrow model makes the assumption of V-cavities that cannot represent actual physical surfaces. One of the most used representations [10,11,25] has been proposed by Smith [29], making the assumption of a separable form, so that masking and shadowing are independent:

$$G(\mathbf{i}, \mathbf{o}, \mathbf{m}) = G_1(\mathbf{i}, \mathbf{m})G_1(\mathbf{o}, \mathbf{m}). \quad (16)$$

Given that the GAF should be independent from the normal \mathbf{m} of a microfacet, i.e. $G_1(\mathbf{u}, \mathbf{m})$ does not correlate with any other microfacet, even nearby, it leads to the following expression:

$$G_1(\mathbf{u}, \mathbf{m}) = \begin{cases} G_1(\mathbf{u}) & \text{when } \mathbf{u} \cdot \mathbf{m} > 0 \\ 0 & \text{when } \mathbf{u} \cdot \mathbf{m} \leq 0, \end{cases} \quad (17)$$

with

$$G_1(\mathbf{u}) = \frac{\mathbf{u} \cdot \mathbf{n}}{\int_{\Omega_u^+} D(\mathbf{m})|\mathbf{u}\mathbf{m}|d\omega_m}. \quad (18)$$

Ashikhmin *et al.* [10] suggest a prior numerical integration for all directions \mathbf{u} . In the case of Beckmann distribution, this integral has an analytical expression [25] with $G_1(\mathbf{u}) = 1/(1 + \Lambda(\mathbf{u}))$, where:

$$\Lambda(\mathbf{u}) = \frac{\operatorname{erf}(a) - 1}{2} + \frac{1}{2a\sqrt{\pi}}e^{-a^2}, \quad (19)$$

and $a = 1/(\alpha_u \tan \theta_u)$, $\alpha_u = \sqrt{\sigma_x^2 \cos^2 \varphi_u + \sigma_y^2 \sin^2 \varphi_u}$. In the remainder of this paper, we will make the distinction between Gaussian and Beckmann distributions as described in the two previous paragraphs, although Beckmann also corresponds to a Gaussian.

GGX distribution, described in [11,30], has been extended to anisotropic distribution [25]:

$$D(\mathbf{m}) = \frac{1}{\pi\alpha_x\alpha_y|\mathbf{m}\mathbf{n}|^4 \left(1 + \tan^2 \theta_m \left(\frac{\cos^2 \varphi_m}{\sigma_y^2} + \frac{\sin^2 \varphi_m}{\sigma_x^2}\right)\right)^2}. \quad (20)$$

The associated GAF is also obtained using $G_1(\mathbf{u}) = 1/(1 + \Lambda(\mathbf{u}))$, with:

$$\Lambda(\mathbf{u}) = \frac{-1 + \sqrt{1 + 1/a^2}}{2}, \quad (21)$$

where $a = 1/(\alpha_u \tan \theta_u)$, $\alpha_u = \sqrt{\sigma_x^2 \cos^2 \varphi_u + \sigma_y^2 \sin^2 \varphi_u}$.

3.3 Light Inter-reflections

Light multiple reflections between microfacet interface and body (Figure 3) are analytically handled by our model (Equations 9 and 8). In addition, light reflections between microfacets should also be accounted for. Equation 2 stands for single-bounce reflections; to the best of our knowledge, multiple-bounce inter-reflections with microfacets have only been handled by Oren and Nayar [9], who consider the influence of two bounces of reflections with pure Lambertian microfacets, under the assumption of V-cavities (Figure 6).

This problem is difficult since it requires to solve the infinite dimensional integral rendering equation. We have implemented a numerical Monte-Carlo integration for estimating light inter-reflections with V-cavities and interfaced Lambertian microfacets given in Equation 4. Given an incident light direction \mathbf{i} , the BRDF is the sum of all the contributions $f^\infty = f^1 + f^2 + \dots$, where f^k corresponds to the observed radiance (or reflectance with unitary irradiance) after k reflections:

$$\begin{aligned} f^\infty(\mathbf{i}, \mathbf{o}, \mathbf{n}) &= \frac{dL^\infty(\mathbf{i}, \mathbf{o}, \mathbf{n})}{|\mathbf{i}\mathbf{n}|} \\ &= \int_{\Omega_+} \frac{R^\infty(\mathbf{i}, \mathbf{o}, \mathbf{m})}{|\mathbf{i}\mathbf{n}|} \frac{|\mathbf{o}\mathbf{m}|}{|\mathbf{o}\mathbf{n}|} D(\mathbf{m})d\omega_m, \end{aligned} \quad (22)$$

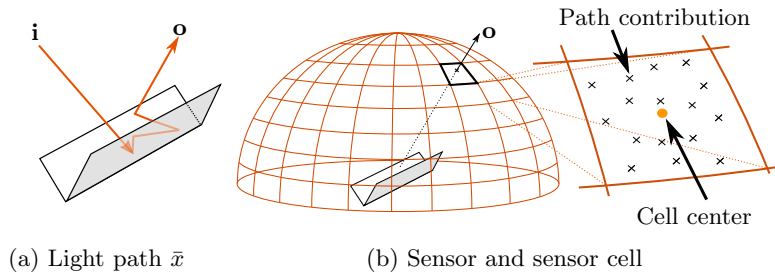


Figure 6: Light inter-reflections within V-cavities: (a) Light path starts using a given direction \mathbf{i} and interacts with the microfacets before exiting in direction \mathbf{o} ; (b) its contribution is collected on a hemispherical sensor subdivided in equal solid angle cells; $f^\infty(\mathbf{i}, \mathbf{o}, \mathbf{n})$ is computed in each cell using density estimation based on all paths contributing to the cell.

where dL^∞ is the total reflected radiance in direction \mathbf{o} for a collimated light beam coming from direction \mathbf{i} . This formulation takes into account all light interactions with all possible microfacets complying with distribution D . $R^\infty(\mathbf{i}, \mathbf{o}, \mathbf{m}) = \int_S L(\bar{x}) d\bar{x}$ is the total reflected radiance for all light paths \bar{x} (from the path domain S and $L(\bar{x})$ is the path contribution function) with at least one bounce inside a V-cavity represented by its normal \mathbf{m} . $L(\bar{x})$ is estimated using path tracing.

We propose to evaluate Equation 22 using Monte-Carlo quadrature. First, a microfacet orientation is chosen according to importance sampling, depending on the *probability density function* (pdf) $D(\mathbf{m})|\mathbf{m}\mathbf{n}|$; second, a point x_i is uniformly chosen on the microfacet; third, a light path is built similarly to the photon mapping rendering method [31], from a randomly chosen direction \mathbf{i} . This path hits the point x_i from direction \mathbf{i} , reflects several times within the V-cavity and finally gets out of the microsurface. The path contribution is collected on a virtual hemispherical sensor, subdivided such that all cells correspond to the same solid angle (Figure 6). With this simulation method, shadowing and masking terms are automatically handled. Moreover, similarly to Oren and Nayar [9], V-cavities are considered as much longer than large.

Inside each sensor cell, density estimation is used to capture $f^\infty(\mathbf{i}, \mathbf{o}, \mathbf{n})$ where \mathbf{o} is the center direction of the cell solid angle:

$$f^\infty(\mathbf{i}, \mathbf{o}, \mathbf{n}) \approx \frac{\sum_{j=1}^N \frac{1}{|\mathbf{i}\mathbf{n}|} L(\bar{x}_j) \frac{|\mathbf{o}_{\bar{x}_j} \mathbf{m}_j|}{|\mathbf{o}_{\bar{x}_j} \mathbf{n}|} D(\mathbf{m}_j)}{N_{tot} \Delta\omega_o}, \quad (23)$$

where N_{tot} is the total number of samples used to estimate Equation 22, N is the number of paths contributing to the cell, $\mathbf{o}_{\bar{x}_j}$ is the outgoing direction of path \bar{x}_j , \mathbf{m}_j is the sampled microfacet normal and $d\omega_o$ the cell's solid angle.

Figure 7 illustrates the effects of taking into account inter-reflections (two and multiple bounces). Simulations are done with one billion light paths and a sensor containing 3240 cells. When the microfacet BRDF is close to Lambertian, inter-reflections play a role in the total reflection model in case of a rough surface. On the other hand, pure specular microfacets produce almost no additional reflected light. Two light bounces are significant for Lambertian microfacets, while further reflections produce only very low additional reflected radiance in most configurations (as already explained in [9]). Some more results can be found in the joined additional material file.

This protocol makes use of V-cavities, with the advantage that it does not require to explicitly construct a surface composed of fixed microfacets, and enables the computation without loss of generality. Using other types of representation complying with Smith's GAF would require some more experiments, which are beyond the scope of this paper.

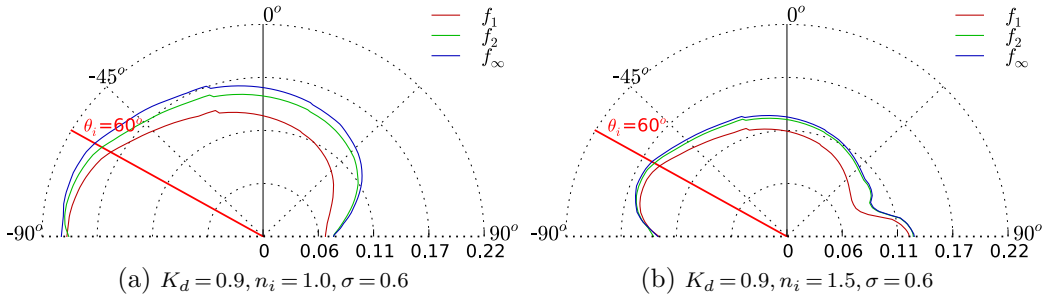


Figure 7: V-cavities reflectance with inter-reflections, Beckmann distribution: f_1 corresponds to a single bounce; f_2 corresponds to the BRDF with two light bounces; f_∞ includes all bounces, using the Russian roulette strategy.

4 BRDF Integration and Sampling

Interfaced Lambertian microfacet BRDFs are composed of two terms f_s and f_b (Section 3.2) that can be processed independently with the rendering equation, due to integration linearity:

$$L_o(x, \mathbf{o}, \mathbf{n}) = \int_{\Omega_+} L_i(x, \mathbf{i}, \mathbf{n}) f(\mathbf{i}, \mathbf{o}, \mathbf{n}) |\mathbf{in}| d\omega_i, \quad (24)$$

where x is the considered surface element location, $L_o(x, \mathbf{o}, \mathbf{n})$ corresponds to the outgoing radiance, $L_i(x, \mathbf{o}, \mathbf{n})$ is the incident radiance, coming from direction ω_i , and $f(\mathbf{i}, \mathbf{o}, \mathbf{n}) = f_s(\mathbf{i}, \mathbf{o}, \mathbf{n}) + f_b(\mathbf{i}, \mathbf{o}, \mathbf{n})$. The glossy term corresponds to the well-known formulation provided by Equation 3, while the body part is directly derived from Equation 2, using the microfacet body contribution f_b^μ (Equation 12):

$$f_b(\mathbf{i}, \mathbf{o}, \mathbf{n}) = \int_{\Omega_+} \frac{|\mathbf{im}|}{|\mathbf{in}|} f_b^\mu(\mathbf{i}, \mathbf{o}, \mathbf{m}) \frac{|\mathbf{om}|}{|\mathbf{on}|} D(\mathbf{m}) G(\mathbf{i}, \mathbf{o}, \mathbf{m}) d\omega_m. \quad (25)$$

Unfortunately, Equation 25 requires numerical integration. The next section shows how it can be handled straightforwardly in any Monte-Carlo rendering system, producing correct results without making use of any approximation. We also provide in this paper an approximate isotropic model, that can be used without Monte-Carlo integration, for instance for GPU applications or data fitting.

4.1 Monte-Carlo Integration

Most renderers based on ray-tracing approaches make use of Monte-Carlo integration for estimating the rendering equation. In those cases, BRDF importance sampling is used for reducing variance, as pointed out by many authors [11, 20, 32, 33].

Sampling BRDFs requires integrating Equation 25 (corresponding to the body contribution), using a stochastic process that only requires choosing microfacet orientations. Although microfacet reflectance and the resulting BRDF are smooth, uniform sampling is not efficient due to the distribution function D that might introduce high frequencies (thin peaks and long tails), resulting in noise. Importance sampling should thus also be used, based on $D(\mathbf{m})|\mathbf{mn}|$, as for path tracing importance sampling.

The specular component (Equation 3) can be processed as in any rendering system, without changing the importance sampling strategy, as it corresponds to the usual Cook-Torrance formulation (with potentially different distributions and/or attenuation factors).

Choosing between surface and body sampling is the first step. Ideally, f_s and f_b should be integrated over hemispherical incidence directions to determine each term weight. However, this process would be inefficient in practice. Instead, we propose to apply the process as for a Lambertian surface with a flat interface (Equations 5 and 8). The resulting analytical formulation depends on

K_d and n_i ; it is physically exact with a plane interface, and this assumption is efficient with rough surfaces since the balance between the two terms remains approximately identical.

Let us define $R_s = r_e$ the total specular reflectance provided by Molenaar, in Equation 11, and the total body reflectance $R_b = \frac{1}{n_i^2}(1-r_e)^2 \frac{K_d}{1-K_d r_i}$; We use the proportion between R_s and R_b for choosing the contribution between specular and body directions. Given a uniform random value $\xi_0 \in [0, 1[$, if $\xi_0 < R_s/(R_s + R_b)$, then sample a specular direction, otherwise, sample a body direction.

Importance sampling the specular/glossy term has been discussed by many authors; Walter *et al.* [11] provide an overview on the subject. Based on the microfacet distribution (see below for an anisotropic representation), the pdf is given by $D(\mathbf{m})|\mathbf{m}\mathbf{n}|$. The weight associated with the outgoing direction is:

$$w(\mathbf{i}) = \frac{f_s(\mathbf{i}, \mathbf{o}, \mathbf{m})D(\mathbf{m})G(\mathbf{i}, \mathbf{o}, \mathbf{m})}{4|\mathbf{i}\mathbf{n}||\mathbf{o}\mathbf{n}|p_o(\mathbf{i})}, \quad (26)$$

with:

$$p_o(\mathbf{i}) = \text{pdf}(\mathbf{m}) \left\| \frac{\partial \omega_h}{\partial \omega_o} \right\| = \text{pdf}(\mathbf{m}) \frac{1}{4|\mathbf{o}\mathbf{m}|}. \quad (27)$$

Body term sampling is more difficult since all microfacet contributions should be accounted for. We propose to transfer BRDF integration in the rendering system directly. The Monte-Carlo process can be applied to the whole rendering equation, including the analytical BRDF:

$$L_o(\mathbf{o}, \mathbf{n}) = \int_{\Omega^+} L_i(\mathbf{i}, \mathbf{n}) \int_{\Omega^+} \hat{f}_b(\mathbf{i}, \mathbf{o}, \mathbf{n})|\mathbf{i}\mathbf{n}|d\omega_m d\omega_i, \quad (28)$$

where $\hat{f}_b(\mathbf{i}, \mathbf{o}, \mathbf{n}) = \frac{|\mathbf{i}\mathbf{m}|}{|\mathbf{i}\mathbf{n}|} f_b^\mu(\mathbf{i}, \mathbf{o}, \mathbf{m}) \frac{|\mathbf{o}\mathbf{m}|}{|\mathbf{o}\mathbf{n}|} D(\mathbf{m})G(\mathbf{i}, \mathbf{o}, \mathbf{m})$, as stated in Equation 25.

This equation exhibits a four dimensional integral that can also be solved according to Monte-Carlo importance sampling. Therefore, the process consists in selecting the incoming direction \mathbf{i} according to a first importance sampling process, based on a pdf equal to $|\mathbf{i}\mathbf{n}|/\pi$, as well as a microfacet orientation \mathbf{m} with on a second importance sampling process based on a pdf equal to $D(\mathbf{m})|\mathbf{m}\mathbf{n}|$. Anisotropy is straightforwardly handled by the chosen distribution of $D(\mathbf{m})$.

Using the anisotropic distributions for Beckmann and GGX (Equations 15 and 20), importance sampling of a single microfacet is given by the following sampling. In the following, (ξ_1, ξ_2) are two uniform random variables in $[0, 1]^2$; the value of φ_m is identically sampled for all distributions:

$$\varphi_m = \arctan \left(\frac{\sigma_y}{\sigma_x} \tan(2\pi\xi_2) \right). \quad (29)$$

The value for θ_m depends on the chosen distribution, reversing the cumulative density function (cdf) associated with $\text{pdf}(\mathbf{m}) = D(\mathbf{m})|\mathbf{m}\mathbf{n}|$.

With the Beckmann distribution:

$$\theta_m = \arctan \left(\sqrt{\frac{-\log(\xi_1)}{\frac{\cos^2 \varphi_m}{\sigma_x^2} + \frac{\sin^2 \varphi_m}{\sigma_y^2}}} \right). \quad (30)$$

With the GGX distribution:

$$\theta_m = \arctan \left(\sqrt{\frac{\xi_1}{(1-\xi_1) \left(\frac{\cos^2 \varphi_m}{\sigma_x^2} + \frac{\sin^2 \varphi_m}{\sigma_y^2} \right)}} \right). \quad (31)$$

Note that importance sampling a Gaussian distribution is not straightforward since the cdf cannot be analytically represented and thus inverted.

5 Results and Discussion

Our model has been added as a plugin to the Mitsuba renderer [34], and the approximate version has been derived as a glsl shader. Table 2 provides the configurations of distributions and attenuation factors we have used in this paper. In the following tables and figures, IL refers to our interfaced Lambertian microfacets.

Table 2: Configurations of distributions and attenuation factors used in this paper.

Notation	Distribution (D)	Attenuation factor (G)
Gauss, TS	Gaussian normals	Torrance-Sparrow
Beckm, TS	Beckmann (slopes)	Torrance-Sparrow
Beckm, SB	Beckmann (slopes)	Smith-Bourlier
GGX	GGX	GGX GAF

Influence of interface on body reflection is illustrated in Figure 8, according to the choice of functions $D(\mathbf{m})$ and $G(\mathbf{m})$. The discontinuity corresponding to the Torrance-Sparrow GAF V-cavities essentially influences the BRDF at grazing incidence and/or observation angles. In addition, when σ is low and/or when n_i is close to 1, the difference between Torrance-Sparrow and Smith GAFs tends to decrease. Note that the higher tail for GGX distribution produces increasing values at grazing observation angles (Figure 8.c).

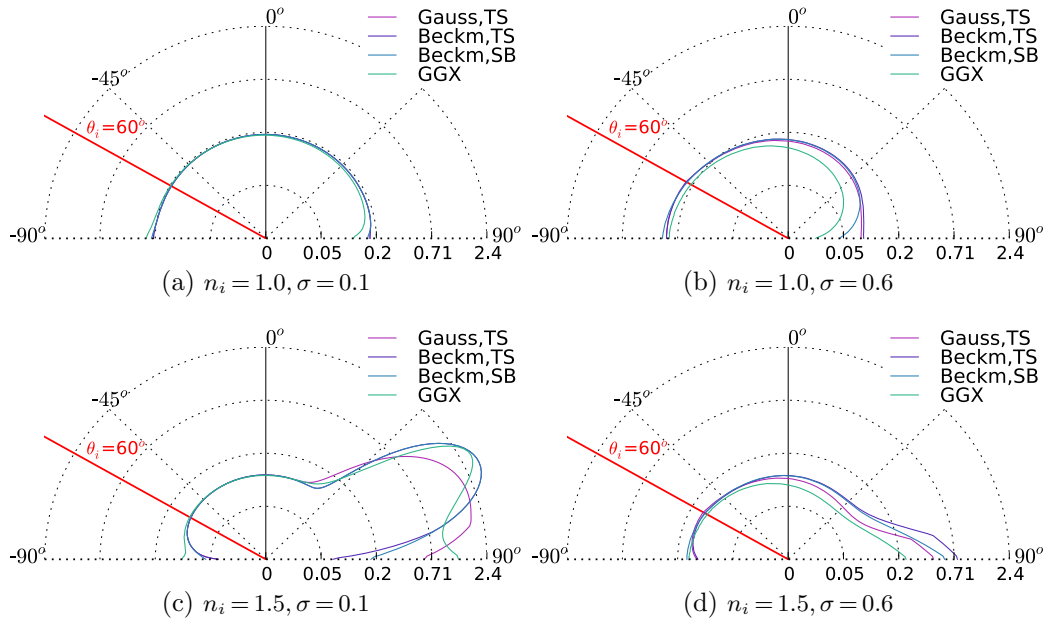


Figure 8: Influence of distributions and GAFs for several values of n_i and σ , illustrated for $\theta_i = 60^\circ$ (log scale).

Rough interfaced Lambertian materials can be compared with combinations of existing models; the closest configuration would be Oren-Nayar’s (Gaussian distribution and Torrance-Sparrow GAF) for the body component and Cook-Torrance’s formulation using the same distribution and GAF. Figure 9 illustrates this configuration, the curves exhibit a new behavior with interfaced Lambertian microfacets, which does not correspond to a Lambertian surface, nor to Lambertian microfacets.

Monte-Carlo rendering results are also provided, using path tracing. Figures 10 and 11 illustrate rendered images with isotropic materials associated to two objects in the scene with various values of n_i and σ . Anisotropic materials can be rendered with the same method, as shown in Figure 12. Note that even with $n_i = 1.0$ (Lambertian microfacets), anisotropy remains visible.

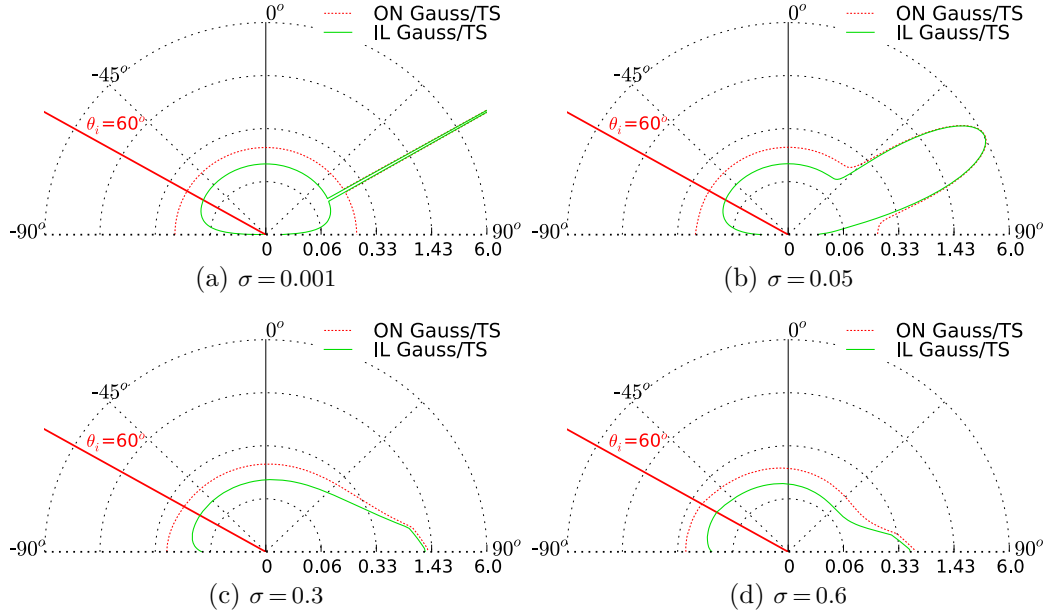


Figure 9: Comparison between Oren-Nayar coupled with specular microfacets (Gaussian distribution and Torrance-Sparrow GAF) and interfaced Lambertian (IL, same distribution and GAF), with $K_d=0.6$, $n_i=1.5$, and various values of σ (log scale).

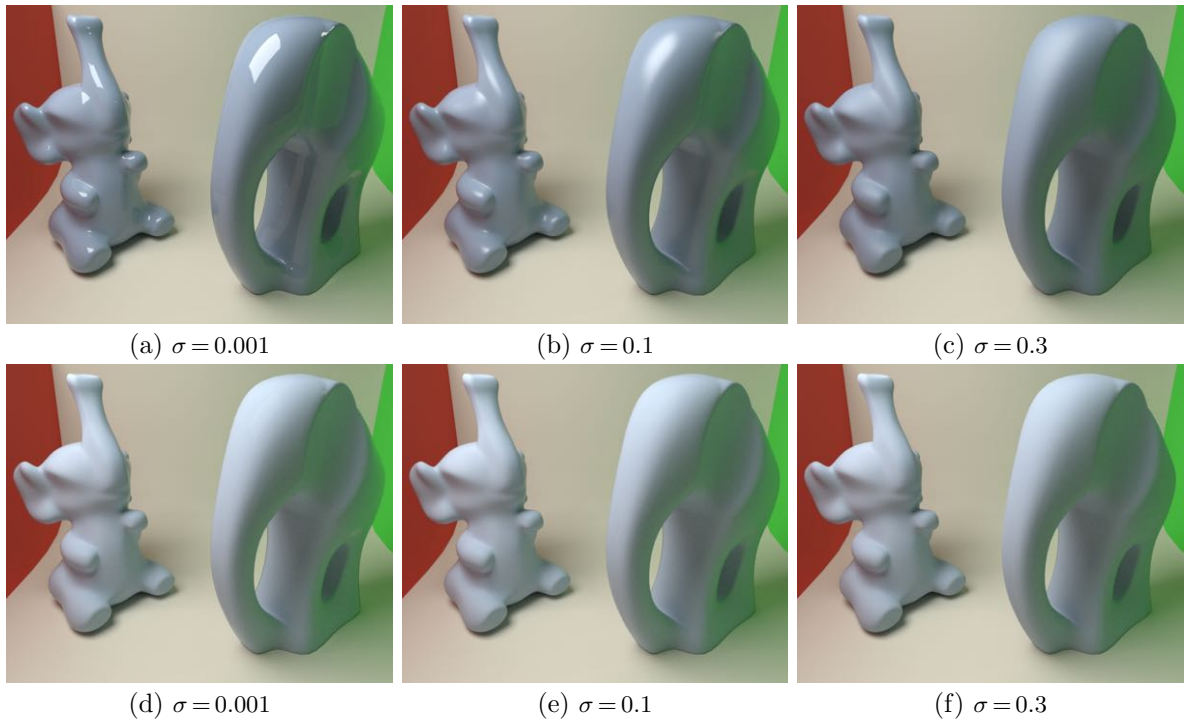


Figure 10: Isotropic IL elephants (with both the same parameters), rendered using path tracing: (top) $n_i=1.5$, for glossy materials and various roughnesses, clearly visible on the specular highlight; (bottom) $n_i=1.1$, with matte objects and backreflections (progressively darkening the right part of the bigger elephant).

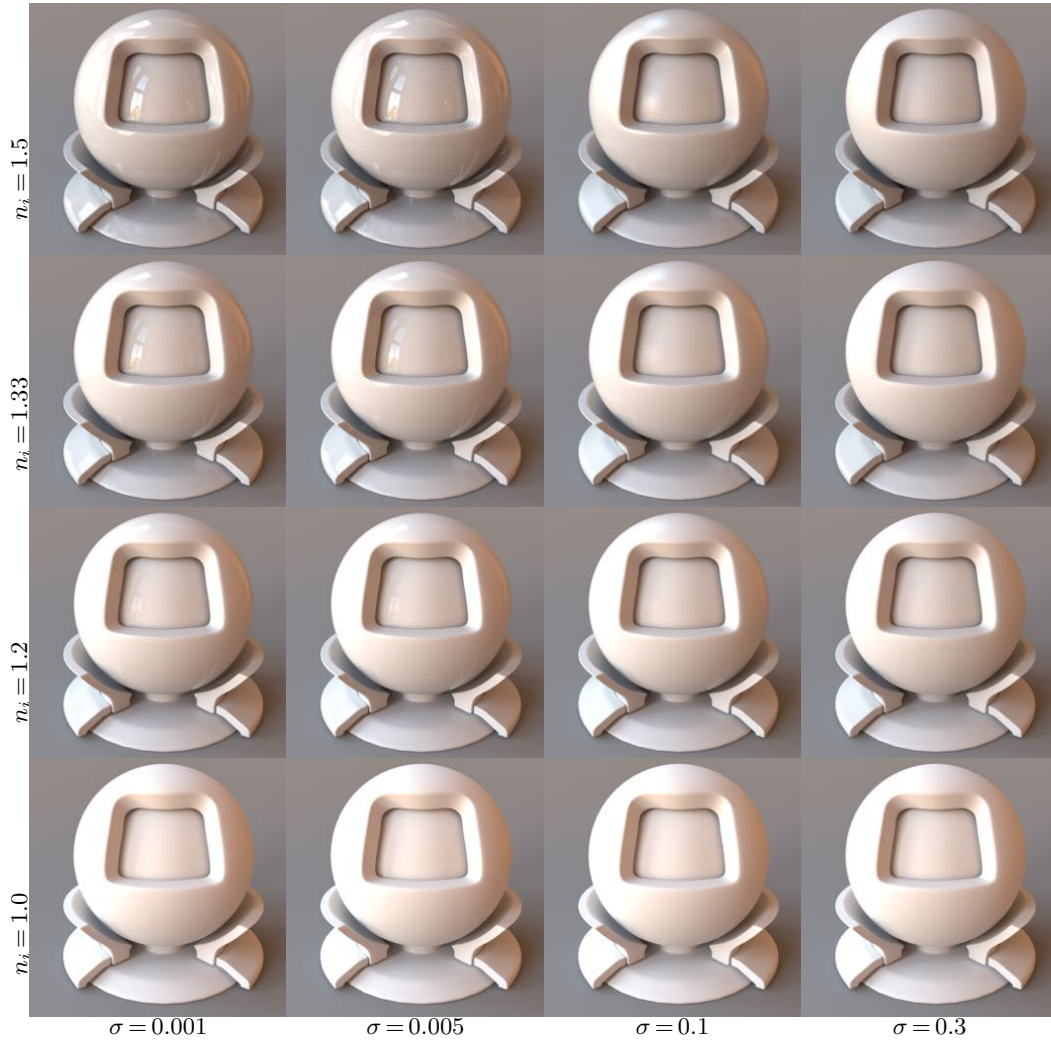


Figure 11: Appearance variations according to n_i and σ , with Beckmann distribution and Smith GAF. The bottom line corresponds to pure Lambertian microfacets, and the bottom-left image is an almost flat Lambertian surface.

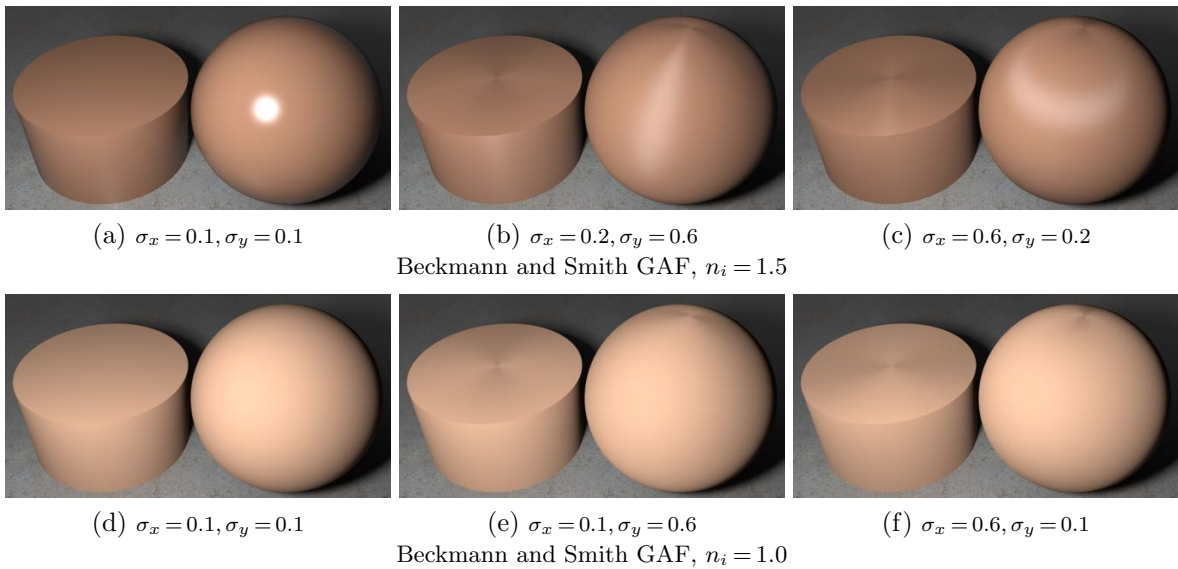


Figure 12: Anisotropic interfaced Lambertian microfacets, with (top) $n_i = 1.5$ and (bottom) $n_i = 1.0$.

6 Conclusion

This paper presents an analysis and implementation methods for interfaced Lambertian microfacet BRDFs. The presented model relies on very few parameters (refractive index, substrate reflectance and surface roughness) and generalizes the Lambert model, as well as specular microfacets and Lambertian microfacets. It is physically plausible and can be straightforwardly integrated in any Monte-Carlo-based rendering system using importance sampling with any distribution and geometric attenuation factor. The proposed methodology can be extended to any type of microfacet-based reflectances.

We have also proposed an approximate version (corresponding to two distributions) of this model that can be employed with interactive rendering systems, or fitting BRDF data, for avoiding numerical integration that remains time consuming. It also integrates light inter-reflections between microfacets.

Our model and the methods we propose in this paper do not correspond to a subset of Jakob *et al.*'s approach [12] due to the interface management which is different from multi-layers; for instance, pure Lambertian microfacet BRDFs are inherently included in our model, and no light simulation between layers is required.

A limitation of our method concerns the mean to estimate light inter-reflections between microfacets. The corresponding contributions are handled by our approximate model, with V-cavities approximations, but including this computation within path tracing remains a difficult issue, a deeper analysis would be needed.

An interesting question concerns the correlation between the interface and the substrate roughnesses, since a single-roughness value constrains both specular peaks and body reflection, which is not always observed in measured materials. We also wish to investigate such a representation.

References

- [1] B. T. Phong, "Illumination for computer generated pictures," *Communications of the ACM*, vol. 18, no. 6, pp. 311–317, 1975.
- [2] J. F. Blinn, "Models of light reflection for computer synthesized pictures," in *ACM SIGGRAPH*, 1977, pp. 192–198.
- [3] R. R. Lewis, "Making shaders more physically plausible," in *Eurographics Workshop on Rendering*, 1993, pp. 47–62.
- [4] L. Claustres, M. Paulin, and Y. Boucher, "BRDF measurement modelling using wavelets for efficient path tracing," *Computer Graphics Forum*, vol. 22, no. 4, pp. 701–716, 2003.
- [5] S. Westin, J. Arvo, and K. E. Torrance, "Predicting reflectance functions from complex surfaces," in *ACM SIGGRAPH*, 1992, pp. 255–264.
- [6] E. P. F. Lafortune, S.-C. Foo, K. E. Torrance, and D. P. Greenberg, "Non-linear approximation of reflectance functions," in *ACM SIGGRAPH*, 1997, pp. 117–126.
- [7] R. L. Cook and K. E. Torrance, "A reflectance model for computer graphics," *ACM Transactions on Graphics*, vol. 1, no. 1, pp. 7–24, Jan. 1982.
- [8] G. J. Ward, "Measuring and modeling anisotropic reflection," in *ACM SIGGRAPH*, 1992, pp. 265–272.
- [9] M. Oren and S. K. Nayar, "Generalization of Lambert's reflectance model," in *ACM SIGGRAPH*, 1994, pp. 239–246.
- [10] M. Ashikhmin, S. Premoze, and P. Shirley, "A microfacet-based BRDF generator." in *ACM SIGGRAPH*, 2000, pp. 65–74.

- [11] B. Walter, S. R. Marschner, H. Li, and K. E. Torrance, “Microfacet models for refraction through rough surfaces,” in *Eurographics Symposium on Rendering*, 2007.
- [12] W. Jakob, E. D’Eon, O. Jakob, and S. Marschner, “A comprehensive framework for rendering layered materials,” *ACM SIGGRAPH*, vol. 33, no. 4, 2014.
- [13] M. Kurt, L. Szirmay-Kalos, and J. Křivánek, “An anisotropic brdf model for fitting and monte carlo rendering,” *ACM SIGGRAPH*, vol. 44, no. 1, pp. 3:1–3:15, Feb. 2010.
- [14] F.-K. Wu and C. wen Zheng, “Microfacet-based interference simulation for multilayer films,” *Graphical Models*, vol. 78, pp. 26 – 35, 2015.
- [15] K. E. Torrance and E. M. Sparrow, “Theory for off-specular reflection from roughened surfaces,” *Journal of Opt. Soc. Am.*, vol. 57, no. 9, pp. 1105–1114, 1967.
- [16] P. Callet, “Physically based rendering of metallic paints and coated pigments,” in *Visualization and Modelling*, december 1995, pp. 287–301.
- [17] —, “From fundamental optical properties of materials to visual appearance: metals, alloys, gilts, glasses, paints, photonics and biophotonics,” in *VIIIth Color Conference*, 2012, pp. 16–25.
- [18] B. van Ginneken, M. Stavridi, and J. J. Koenderink, “Diffuse and specular reflectance from rough surfaces,” *Applied Optics*, vol. 37, no. 1, pp. 130–139, Jan 1998.
- [19] A. Kienle and F. Foschum, “250 years lambert surface: does it really exist?” *Opt. Express*, vol. 19, no. 5, pp. 3881–3889, Feb 2011.
- [20] C. Kelemen and L. Szirmay-Kalos, “A microfacet based coupled specular-matte BRDF model with importance sampling,” in *Eurographics (short presentations)*, 2001.
- [21] P. Shirley, H. Hu, B. Smits, and E. Lafortune, “A practitioners’ assessment of light reflection models,” in *PG ’97: Proceedings of Pacific Graphics ’97*, 10 1997.
- [22] L. Simonot, “A photometric model of diffuse surfaces described as a distribution of interfaced Lambertian facets,” *Applied Optics-OT*, vol. 48, pp. 5793–5801, 2009.
- [23] M. Bagher, C. Soler, and N. Holzschuch, “Accurate fitting of measured reflectances using a Shifted Gamma micro-facet distribution,” *Computer Graphics Forum*, vol. 31, no. 4, pp. 1509–1518, 2012.
- [24] J. Dupuy, E. Heitz, J.-C. Iehl, P. Poulin, F. Neyret, and V. Ostromoukhov, “Linear efficient antialiased displacement and reflectance mapping,” *ACM Transactions on Graphics*, vol. 32, no. 6, p. Article No. 211, Nov. 2013.
- [25] E. Heitz, “Understanding the masking-shadowing function in microfacet-based brdfs,” *Journal of Computer Graphics Techniques (JCGT)*, vol. 3, no. 2, pp. 32–91, juin 2014.
- [26] F. E. Nicodemus, J. C. Richmond, J. J. Hsia, I. W. Ginsber, and T. Limperis, *Geometrical consideration and nomenclature for reflectance*. Final Report National Bureau of Standards, Washington, DC. Inst. for Basic Standards., 1977.
- [27] C. Bourlier, G. Berginc, and J. Saillard, “One and two-dimensional shadowing functions for any height and slope stationary uncorrelated surface in the monostatic and bistatic configurations,” *IEEE Transactions on Antennas and Propagation*, pp. 312–324, 2002.
- [28] R. Molenaar, J. J. ten Bosch, and J. R. Zijp, “Determination of kubelka-munk scattering and absorption coefficients by diffuse illumination,” *Applied Optics*, vol. 38, no. 10, pp. 2068–2077, Apr 1999.
- [29] B. Smith, “Geometrical shadowing of a random rough surface,” *IEEE Transactions on Antennas and Propagation*, pp. 668–671, 1967.
- [30] T. S. Trowbridge and K. P. Reitz, “Average irregularity representation of a rough surface for ray reflection,” *Journal of Opt. Soc. Am.*, vol. 65, no. 5, pp. 531–536, May 1975.

- [31] H. W. Jensen, *Realistic Image Synthesis Using Photon Mapping*. Natick, MA, USA: A. K. Peters, Ltd., 2001.
- [32] E. Lafortune, “Mathematical models and monte carlo algorithms for physically based rendering,” Ph.D. dissertation, Katholieke Universiteit Leuven, 1996.
- [33] E. Veach, “Robust monte carlo methods for light transport simulation,” Ph.D. dissertation, Stanford University, 1998.
- [34] W. Jakob, “Mitsuba renderer,” 2010, <http://www.mitsuba-renderer.org>.